5th Intern. Conference "The Science of making torque from wind, TORQUE, Copenhagen, 2014

Reduction of airfoil trailing edge noise by trailing edge blowing

T Gerhard[1,3], S Erbslöh[2] and T Carolus[1]

[1]Institute for Fluid- and Thermodynamics, University of Siegen, 57068 Siegen, Germany
[2]Team Leader Aerodynamics, Senvion SE, 24783 Osterrrönfeld, Germany
[3]Corresponding author; tom.gerhard@uni-siegen.de

Abstract. The paper deals with airfoil trailing edge noise and its reduction by trailing edge blowing. A Somers S834 airfoil section which originally was designed for small wind turbines is investigated. To mimic realistic Reynolds numbers the boundary layer is tripped on pressure and suction side. The chordwise position of the blowing slot is varied. The acoustic sources, i.e. the unsteady flow quantities in the turbulent boundary layer in the vicinity of the trailing edge, are quantified for the airfoil without and with trailing edge blowing by means of a large eddy simulation and complementary measurements. Eventually the far field airfoil noise is measured by a two-microphone filtering and correlation and a 40 microphone array technique.
Both, LES-prediction and measurements showed that a suitable blowing jet on the airfoil suction side is able to reduce significantly the turbulence intensity and the induced surface pressure fluctuations in the trailing edge region. As a consequence, trailing edge noise associated with a spectral hump around 500 Hz could be reduced by 3 dB. For that a jet velocity of 50% of the free field velocity was sufficient. The most favourable slot position was at 90% chord length.

1. Introduction

The ongoing expansion of onshore wind energy results in stricter noise regulations for modern wind turbines. A sound reduced operation of a standard turbine impacts its yield significantly. Hence, a key topic of actual research activities is aero-acoustically generated sound due to the interaction of the flow with the aerodynamically effective surface, i.e. the rotor blade. As, for instance, indicated by Roger [1], the scattering of the turbulent boundary layer at the airfoil trailing edge (TE) acts as the dominant sound source of airfoils in a temporally and spatially homogeneous flow. In general this sound mechanism is called trailing edge noise (TEN). Oerlemans [2] investigated the main airfoil noise sources of six different wind turbine airfoils experimentally in an aeroacoustic wind tunnel with an advanced microphone array technique. Furthermore, with a similar technique, Oerlemans et al. [3] determined the acoustic properties of a full scale turning wind turbine. Both studies proved that the blade TE region is indeed the main contributor to airfoil self noise.

Different approaches exist targeting at the mitigation of the TEN mechanism directly. A traditional rule is to design the TE as thin as possible to avoid so called blunt trailing edge noise (see e.g. Blake and Gershfeld [4], Shannon and Morris [5]) which is now readily done and achievable with standard production techniques. Modifications of the blade TE material (e.g. porous TEs, see Geyer et al. [6]), or the blade TE geometry by serrations, slits or brushes were utilized to diminish TEN passively, see for instance Finez et al. [7], Oerlemans et al. [8] and Herr [9]. Those mitigation techniques provide

TEN reduction mainly as a result of a modified surface impedance. Furthermore, the retrofitting of TE add-ons is critical because the increase of the effective chord length may imply higher blade loads.

By contrast, active trailing edge blowing (TEB) or suction can affect the primary reason for TEN, the unsteady flow created upstream of the TE in the turbulent boundary layer. For practical reasons suction is not an option since the sucking openings may be blocked by dirt during standard operation. This can be avoided by blowing clean air through narrow openings from the blade interior to the outside. Most common applications of TEB are targeting the airfoil resp. rotor aerodynamics in terms of circulation control and lift enhancement, see e.g. Tongchitpakdee et al. [10], Shires et al. [11]. TEB for acoustic reasons was predominantly investigated in the context of turbofan engine noise reduction. Main objective was the mitigation of the rotor-stator interaction noise by filling the wake deficit downstream of the rotor resp. stator in a fan stage. Fite et al. [12] showed that blowing air from the blade TEs of a turbofan rotor provided a tonal noise reduction of up to 6 dB and a broadband noise reduction of appr. 1.5 dB. More recent studies were carried out by Winkler et al. [13] and Kohlhaas et al. [14]. Winkler was focusing on broad band noise reduction from an isolated airfoil and a tandem airfoil assembly. He investigated various slot geometries and confirmed a beneficial effect on broad band noise. Kohlhaas completely eliminated the first harmonic of blade passing frequency sound of a fan stage by optimizing the spanwise blowing profile. In all cases the high frequency blowing self noise acted as a limiting factor of noise reduction by TEB (see also Howe [15]).

The objective of this paper is to revisit broad band TEN from an isolated airfoil and its reduction by TEB. As a generic example a 2D section of a S834 airfoil, which was originally designed by Somers [16] for small and quiet horizontal axis wind turbines, is investigated in this study. In detail we are focussing on the unsteady flow in the vicinity of the TE, more specifically on the turbulent boundary layer and how it is affected by a blowing jet from a slot located on the airfoil suction side. Since the strength of the radiated noise is related to the turbulence encountering the TE region, the aim is a reduction of the turbulent velocity fluctuations in the boundary layer and hence a decrease of the induced surface pressure fluctuations.

2. Methodology

2.1. Airfoil Section

The S834 airfoil section investigated has a chord length of $c = 0.2$ m and an aspect ratio of 1.33. It is mounted between sideplates in an open wind tunnel, $0.5 \cdot c$ downstream of the nozzle exit. The effective angle of attack (AOA) α_{eff} is chosen such that an infinite aspect ratio section of this airfoil would operate at its optimal lift to drag ratio for a chord based Reynolds number $Re = 3.5 \cdot 10^6$, i.e. $\alpha_{eff} = 4.7°$. To compensate for open wind tunnel installation effects, a correction as derived by Brooks et al. [17] is applied, resulting in a geometric AOA of $\alpha_{geom} = 12.7°$ for this particular aspect ratio. However, the available small aeroacoustic wind tunnel provides a maximum flow velocity corresponding to $Re = 3.5 \cdot 10^5$ only. To mimic the 10-times higher target Reynolds number the location of boundary layer transition on pressure and suction side were controlled by a zigzag tape. The tripping locations were selected such that they correspond to the chordwise locations of natural transition for the S834 airfoil at $Re = 3.5 \cdot 10^6$. The locations of natural transition were found via the airfoil performance prediction tool XFOIL [18]. XFOIL yields overall airfoil characteristics as a function of airfoil shape, AOA, Reynolds and Mach number in an undisturbed flow. It is based on a linear-vorticity 2nd order accurate panel method coupled with an integral boundary layer method and an e^n-type transition amplification formulation [19] and allows a prediction of the transition locations. For our case, transition must occur at $x/c = 0.17$ on the airfoil suction side (SS) and at $x/c = 0.76$ on the pressure side (PS), figure 1 (left). All investigations were carried out at a Mach-number of $M = 0.075$.

2.2. *Trailing Edge Blowing Airfoils*

Four configurations of airfoils were investigated: The unmodified S834 airfoil as a reference, and three airfoils equipped with different TEB geometries, figure 1 (right). The blowing slots are located

on the suction side at *x/c* = 0.75, 0.825 and 0.9, respectively. Hence, the three TEB airfoils are labeled TEB 75, TEB 82.5 and TEB 90. These locations of the blowing slots are chosen such that the jet merges in a differently developed boundary layer: At 75% *c* the boundary layer is still rather thin, where at 90% *c* it is thick and the slope of the boundary layer thickness reaches a maximum gradient. Furthermore, by the chordwise variation of the location of the slots, the area between slot and trailing edge is varied which has a potential impact on the sound radiated.

In contrast to many earlier TEB studies, we are not confining ourselves to a momentumless wake. It is rather a question of identifying the acoustically optimal blowing rate concerning the airfoil self noise emissions. Furthermore, one has to keep in mind that the jet self noise increases with increasing blowing rates and may counteract the acoustic benefit of modifications of the turbulent boundary layer by TEB (see e.g. Winkler et al. [13] or Howe [15]). The ejected momentum in terms of the blowing rate is defined as

$$u_b = u_{jet} / u_\infty , \tag{1}$$

with the ejected air velocity u_{jet} and the freestream velocity u_∞. The geometry of the internal slot and the shape of the airfoil contour downstream of the slot have been developed utilizing 2D steady-state, incompressible Reynolds-averaged Navier-Stokes (RANS) simulations with the airfoil being placed in an effectively unbounded and undisturbed flow. One design target was to enable the jet even for $u_b < 1$ to follow the airfoil contour by virtue of the Coandă-effect. The slot height h_s is 1% *c* for all three airfoils and constant in spanwise direction.

The reference airfoil and the front part of the TEB airfoils is CNC-milled from one piece of aluminium, the rear parts of the TEB airfoils are manufactured using a rapid-prototyping technique. This enables the realisation of the different blowing slot geometries while keeping the complex internal air distributing tubing.

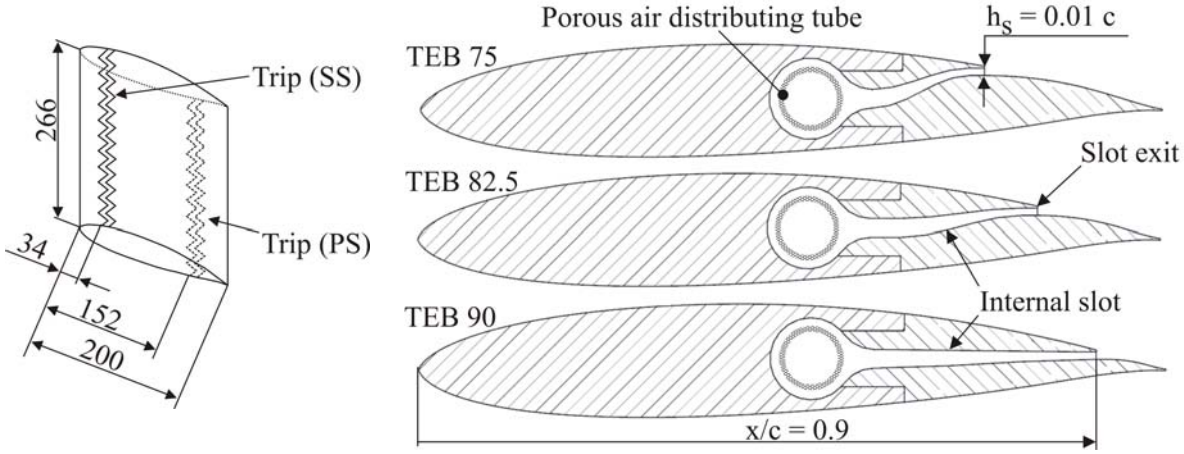

Figure 1. Left: Sketch of the S834 airfoil section with trip positions (dimensions in mm, not to scale); right: Cross-sectional view of the three TEB airfoils (not to scale).

2.3. *Experimental Test Rig and Data Acquisition*

The ejected mass flow rate is controlled via a pneumatic circuit incorporating an external pressure source, a proportional pressure valve and a mass flow meter (ABB Sensyflow FMT200-ECO2), figure 2 (right). The pressurized air is fed into the airfoil section from both sides and distributed via a porous pressure tube towards the internal slot. Two external silencers attenuate extraneous noise emanating from the pressurized air supply system.

The wind tunnel (for details see Winkler and Carolus [20]) exhausts in a semi-anechoic chamber (4.5 m x 3.23 m x 2.9 m) which allows acoustic measurements according to ISO 3745 [21] down to 125 Hz. The characteristic turbulence intensity in a plane 0.01 m downstream of the wind tunnel nozzle exit is 0.2%. The sound from the airfoil sections was measured synchronously by two

microphones (1/2" Brüel & Kjaer™, type 4190), located on pressure and suction side perpendicular to the TE and outside of the flow in a distance of 1.5·*c*, figure 2 (left). The microphones were equipped with a wind screen to avoid any flow induced pseudo sound. In addition to this local sound pressure measurement technique a microphone array (CAE Noise Inspector™) was utilized. The array consists of 40 condenser microphones which are spread over a plane area of 0.5 m^2, figure 3 (left).

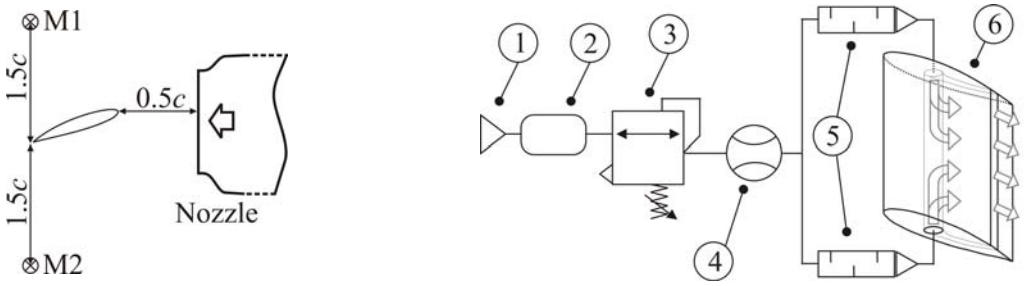

Figure 2. Left: Sketch of the airfoil section and the microphone positions (top view);
right: Schematic layout of the pneumatic circuit with 1 - pressure source, 2 - compressed air reservoir, 3 - proportional pressure valve, 4 - mass flow meter, 5 - silencer, 6 - TEB airfoil.

Since the surface pressure fluctuations in the TE region are acoustically relevant, one rapid-prototyping TE was instrumented with nine flush mounted miniature pressure transducers (Knowles Acoustics, FG-3329-P07), figure 3 (right). This arrangement of sensors allowed the synchronous determination of the stream- and spanwise unsteady pressure distribution in the TE region. Basically these transducers are miniature condenser microphones with a sensitive diameter of 0.7 mm. They have been calibrated in-situ with a white noise excitation signal ranging from 100 Hz to 10 kHz.

Flow velocity and turbulence parameters in the airfoil boundary layer were measured with a 1-D hot-wire anemometer (HWA) (TSI™, type: 1210-T1.5). The probe is operating in a constant-temperature mode using the Streamline™ unit from Dantec Dynamics. For the exact positioning of the probe a three-axes traverse system was used.

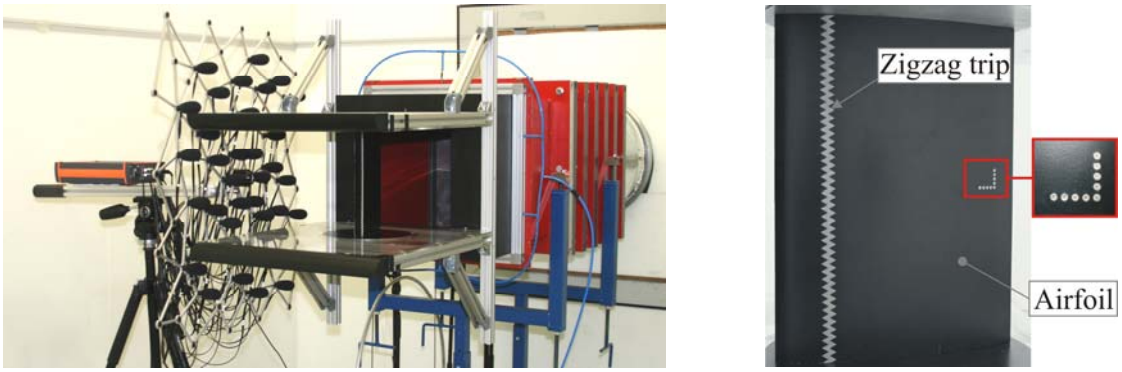

Figure 3. Left: Microphone array next to airfoil;
right: Field of miniature pressure transducers in the TE region (reference airfoil).

2.4. *Acoustic Signal Processing Techniques*

The acoustic signature from the airfoils is relatively low level and potentially contaminated by extraneous sound sources. To isolate the airfoil self noise from ambient sound sources, we take advantage of the fact that the overall airfoil self noise is dominated by the noise emissions occurring at the TE. The dipole characteristic of TEN offers the application of a filtering technique derived by Blake and Lynch [22]. The signals of the two TE phased-matched microphones (M1 and M2 in figure 2, left) should be equal in magnitude but 180° out of phase. The preparatory work is done by a 1st filter that removes all frequency components for which the level of the cross-spectral density (CSD) is less the 6 dB above the background CSD level. The 2nd filter rejects all frequencies where the phase shift

of the CSD is not within a range of 180°±9°. Upon applying both filters, the spectrum contains theoretically pure dipole sound resp. TEN. The emitted free field sound pressure is then specified not as the sound pressure level of a single microphone but as the filtered CSD level of the two adjacent TE microphones L_{Spp}.

Furthermore, the standard microphone measurements are supplemented by microphone array measurements allowing the detection and quantification of the main airfoil sound emitting region also at low signal-to-background noise ratios. For the low frequency range (f < 600 Hz) near field holography was applied. For that the array was positioned 0.25 m next to the airfoil suction side surface. At frequencies above 1000 Hz the Clean SC [23] algorithm was used. Then the array was positioned at a distance of 0.75 m next to the airfoil suction side surface.

With exception of the microphone array all unsteady quantities were captured with a sampling frequency f_s = 51.2 kHz. The spectral analysis is based on the power spectral density obtained by the *pwelch* routine in MATLAB® Vers. 2012a (Δf_{ref} = 1 Hz, $p_0 = 2 \cdot 10^{-5}$ Pa, f_0 = 1 Hz). The sampling rate for all 40 microphones from the microphone array was 48 kHz with 24 bits resolution.

2.5. *Numerical Set Up*

A variety of flow simulations were carried out. Key results were obtained from a large eddy simulation (LES) in the vicinity of quasi-3D airfoil elements, figure 4 (right). The boundary conditions of the LES computational domain were taken from a preceding fully turbulent RANS-simulation covering a domain that included the wind tunnel nozzle, the complete reference airfoil section with side plates and the large (anechoic) chamber, in which the wind tunnel exhausts, figure 4 (left). This simulation is named case A.

The RANS-predicted velocities were taken as boundary conditions at the inlet and side planes of the LES domain, in spanwise direction periodic boundary conditions were defined, the outlet was a pressure outlet. The 3D-block-structured numerical grid consists of $8.5 \cdot 10^6$ cells for the reference and $11 \cdot 10^6$ cells for TEB airfoils, with an averaged local grid spacing of about $\Delta x^+ \approx 70$, $\Delta y^+ \approx 0.4$, $\Delta z^+ \approx 30$. The wall-resolving LES utilized a wall adaptive local eddy viscosity (WALE) subgrid-scale model by Nicoud and Ducros [24] and a dimensionless time step-size based on freestream velocity and chord length of $\Delta t = 6.4 \cdot 10^{-4}$. The convective Courant-Friedrichs-Lewy number exceeded only locally the value 1. The flow solver is based on a finite volume method and 2nd order accurate in space and time. For the time integration a bounded 2nd order implicit spatial scheme was used, the spatial integration was done by a bounded central differencing scheme. The achieved residuals of all variables are $1 \cdot 10^{-6}$. The simulations ran for appr. 15 flow-through times. The applied tripping was taken into account as an equivalent step with the height and an average length of the experimentally used zigzag tape, figure 5. The required mass flow rate for the jet of the TEB airfoils was considered in terms of a constant velocity boundary condition at the inlet of the internal slot. The commercial Navier-Stokes code ANSYS FLUENT™ version 14.5 has been used throughout this study. Table 1 summarizes the details of the cases analyzed numerically.

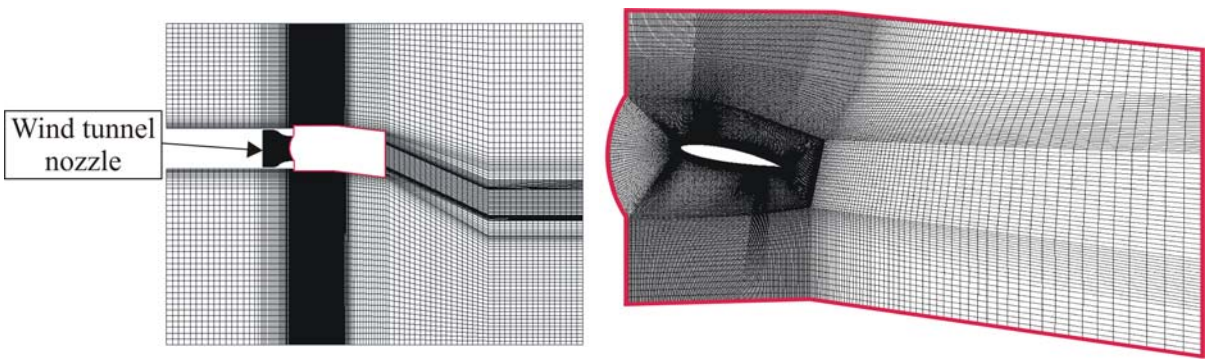

Figure 4. Computational domain and grid topology for preceding RANS of complete set up (case A, left) and for LES of the airfoil section (case B-D, right); only every 2nd mesh line is drawn

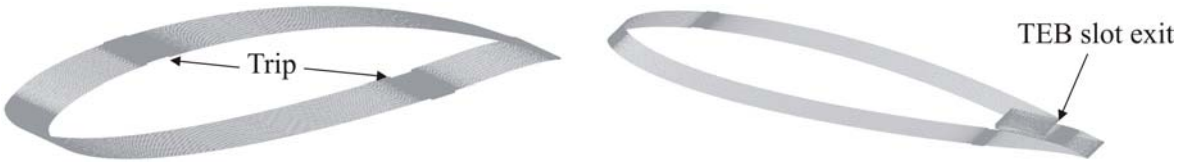

Figure 5. Numerical surface grid of the airfoil element; case A (reference, left) and case B (TEB 90).

Table 1. Simulated cases

Case	Airfoil (Num. method)	Domain	Boundary Conditions Inlet	Outlet	α_{geom} (α_{eff})	u_b	Turbulence/Transition modelling	Grid nodes
A	Reference (RANS)	Complete anechoic chamber with nozzle, sideplates and airfoil	Constant velocity	Pressure (0 Pa)	12.7° (4.7°)	-	k-ω-SST [25] model / fully turbulent (no transition)	$18{\cdot}10^6$
B	Reference (LES)	3D airfoil segment Streamwise: 5.75c Crosswise: 3c Spanwise: 0.075c	Velocities from A	Pressure (0 Pa)	12.7° (4.7°)	-	Subgrid scale model: WALE [24] / trip modelled as step	$8.5{\cdot}10^6$
C	TEB 90 (LES)	as B	as B	as B	as B	0.5	as B	$11{\cdot}10^6$
D	TEB 82.5 (LES)	as B	as B	as B	as B	as C	as B	as C
E	TEB 75 (LES)	as B	as B	as B	as B	as C	as B	as C

3. Results

3.1. *Turbulent boundary layer in the TE region*

A first hint whether TEB could possibly act as a TEN reduction method can be derived from the impact of the ejected jet on the turbulent boundary layer in the TE region. Figure 6 (upper row) shows LES-predicted velocity profiles perpendicular to the surface at four different chordwise positions x/c on the airfoil suction side (y is perpendicular to the wall with $y/c = 0$ at the wall). Note that the TEB blowing rate is always $u_b = 0.5$. The jet becomes clearly visible as it merges in the boundary layer. In general the jet stays very close to the wall, however the increase of the near wall velocity vanishes appr. $0.1{\cdot}c$ downstream of the slot. Furthermore, it is obvious that the boundary layer thickness is increased, even slightly upstream of the slot exit location. This effect can be attributed to the modified geometry and the displacement due to the additionally ejected mass flow.

The lower row in figure 6 shows the turbulence intensity TI in the boundary layer. It is defined as the root-mean-square of the local velocity fluctuations normalized on the freestream velocity:

$$TI = u'/u_\infty \tag{2}$$

In general, as compared to the non-blowing reference, the TEB jet reduces TI in the vicinity of the wall. This effect, however, is limited to a certain range from the blowing slot because a new turbulent boundary layer is developing between jet and wall. It becomes clear that the TEB 90 airfoil provides the largest benefit in the acoustically most relevant trailing edge region among all cases investigated.

Figure 7 shows the validation of the LES results in terms of an exemplary comparison to the experimental measurements. All trends are predicted correctly by the LES, even the quantitative agreement of the LES-prediction is very satisfactory. Note that the flow in the very near-wall region can not be resolved by hot wire anemometry because of the finite probe size.

A second, more relevant indicator for a possible acoustic effect of TEB are the surface pressure fluctuations beneath the turbulent boundary layer in the TE region. Figure 8 clearly proves that the

RMS-value of the fluctuating surface pressure p'_{rms}, here referred to the dynamic freestream pressure p_{dyn}, is decreased considerably by TEB. Depending on the chordwise location of the TEB slot the surface area which benefits from TEB varies. In agreement with the previous observation the TEB 90 configuration provides a surface pressure attenuation nearly down to the TE at $x/c = 1$.

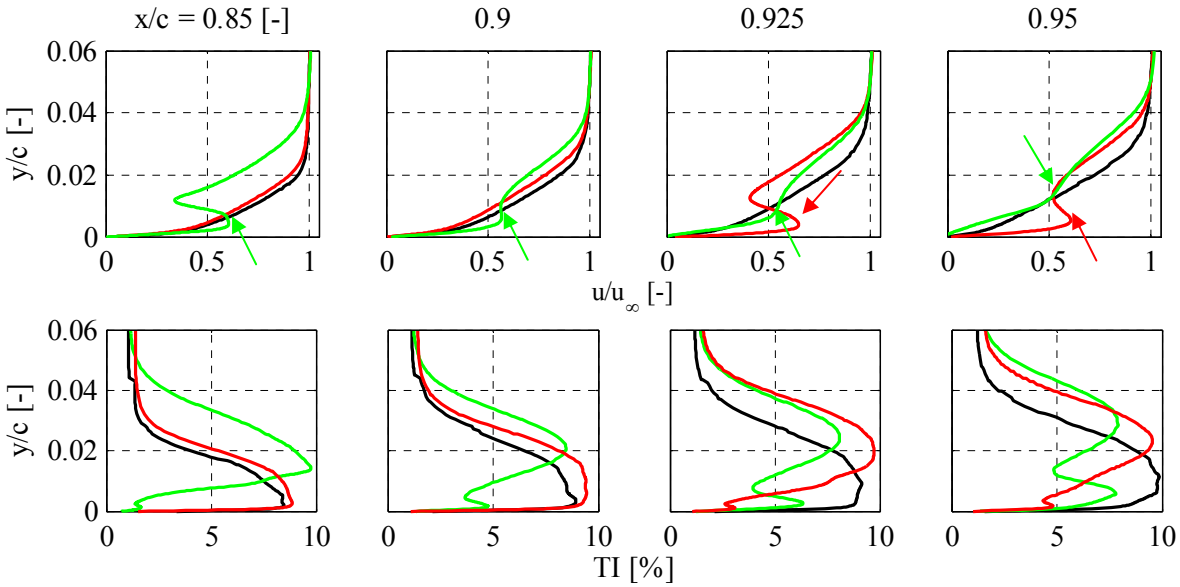

Figure 6. LES-predicted velocity distribution and turbulence intensity in the turbulent boundary layer on the suction side in the TE region, the approximate core of the jets are indicated by an arrow; — case B (reference), — case C (TEB 90), — case D (TEB 82.5).

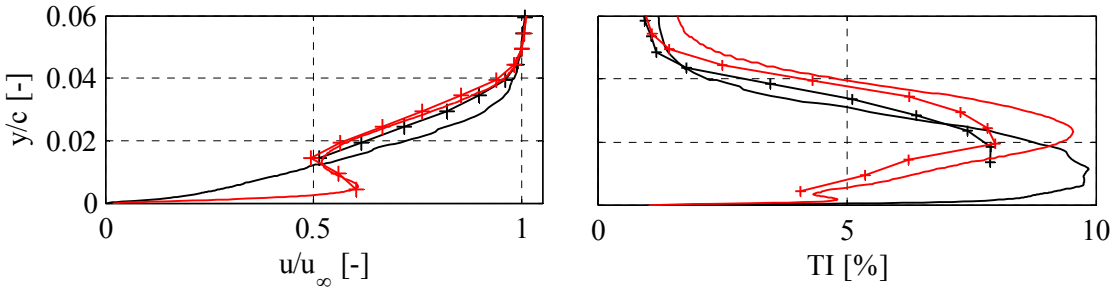

Figure 7. Comparison of LES-predicted and experimentally determined velocity distribution and turbulence intensity in the turbulent boundary layer on the suction side at $x/c = 0.95$; crosses indicate experimental results; — case B (reference), — case C (TEB 90).

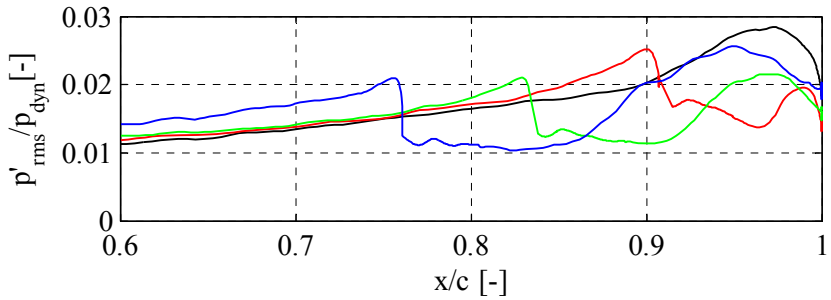

Figure 8. LES-predicted surface pressure fluctuations in the TE region on the suction side; — case B (reference), — case C (TEB 90), — case D (TEB 82.5), — case E (TEB 75).

LES-predicted surface pressure spectra are depicted in figure 9. The TEB jet reduces the pressure fluctuations at lower frequencies while simultaneously increasing the higher frequency components.

On the one hand this effect can be attributed to the destruction of larger and slower turbulent structures containing more energy and contributing to lower frequencies. On the other hand, the jet itself contains smaller turbulent structures feeding energy into the boundary layer at higher frequencies. Furthermore, the increase of the pressure fluctuations upstream of the slot, also visible in figure 8, is due to the scattered boundary layer at the upper edge of the slot. At x/c = 0.95 the TEB 90 airfoil provides a reduction of up to 10 dB at frequencies below 2 kHz. Figure 10 shows the validation of these data by a comparison of the measured and LES-predicted surface pressure spectra at x/c = 0.9 on the reference airfoil suction side. The agreement is not perfect, at frequencies below 2 kHz the level is underpredicted by 5-10 dB. However, the LES shows the tendencies rather well.

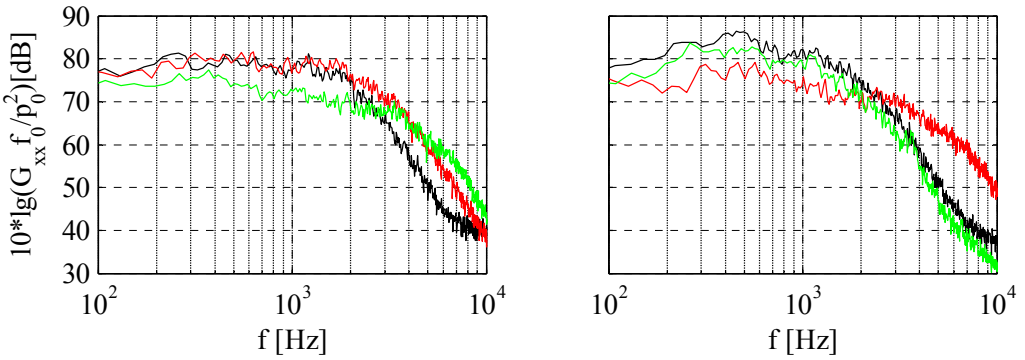

Figure 9. LES-predicted surface pressure spectra at x/c = 0.875 (left) and 0.95 (right), — case B (reference), — case C (TEB 90), — case D (TEB 82.5).

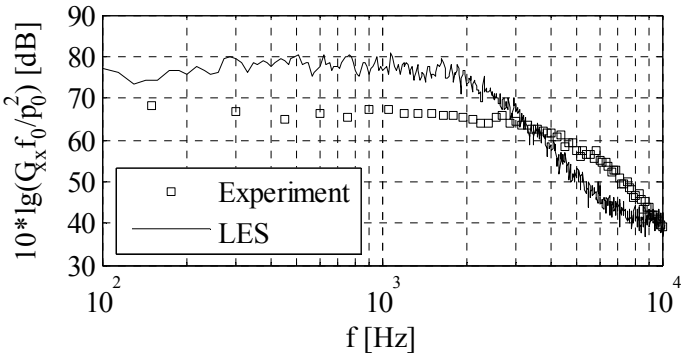

Figure 10. Experimental and LES-predicted surface pressure spectrum (x/c = 0.9; case B, reference).

3.2. Farfield sound

Two questions need to be answered first: (i) What is the characteristic frequency range one can expect TEN in, and (ii) is TEN well above the wind tunnel background noise? As summarized in our previous publication [26], the acoustic evaluations showed the airfoil TE to be the most prominent airfoil self noise source at frequencies from 160 to at least 3000 Hz. Furthermore, one can expect a hump dominating the TEN spectrum to lie in a frequency range between 350 and 550 Hz. Figure 11 shows the measured farfield sound pressure in terms of L_{Spp} ascertained with and without the reference airfoil section present (data processing as described in section 2.4). Between 300 Hz and 3000 Hz, the signal-to-background noise ratio is sufficiently large to identify the radiated airfoil TEN. In figure 12 the sound pressure spectra of the TEB 90 and TEB 82.5 airfoil, again operating at u_b = 0.5, are compared to the reference airfoil spectrum. The TEB 90 airfoil provides a maximum noise reduction of appr. 3 dB in the hump around 500 Hz. The level can be reduced up to $f \approx$ 1.5 kHz until the effect vanishes. The slight increase of the spectral level at frequencies above 3.5 kHz is related to the corresponding spectral components of surface pressure. This confirms the LES results, predicting the largest reduction of *TI* as well as the lowest surface pressure fluctuations in the immediate TE region for TEB 90 airfoil.

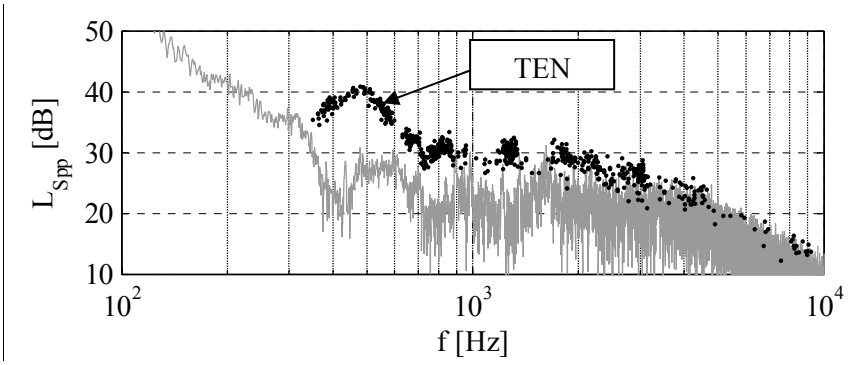

Figure 11. Experimentally determined level of the cross-correlation, airfoil sound against background noise; • case B (reference), — empty wind tunnel (background noise).

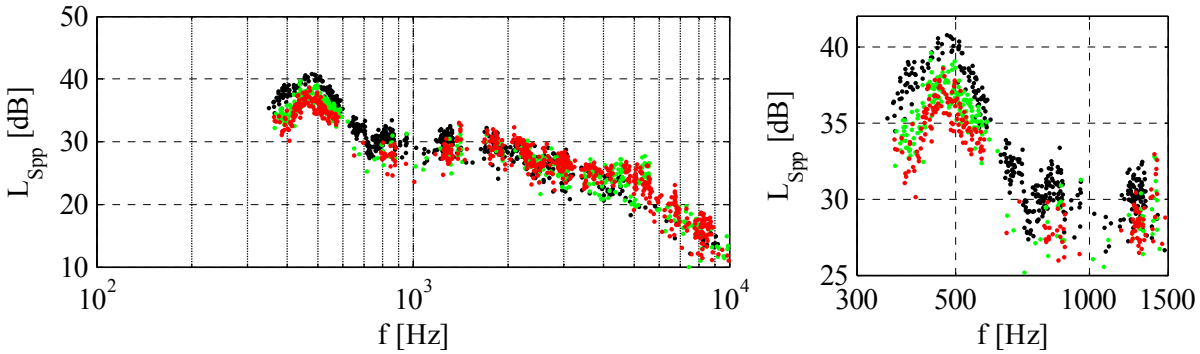

Figure 12. Experimentally determined level of the cross-correlation (right: detailed view on TEN hump); • case B (reference), • case C (TEB 90), • case D (TEB 82.5).

Figure 13 presents the results of the microphone array measurements for the reference and the most promising TEB 90 airfoil in terms of three 1/3-octave frequency bands. In the low frequency band of 250 Hz the airfoil noise is mostly unaffected by TEB. The most significant reduction of about 3 dB is observed in the 400 Hz band. This finding coincides well with the result from the standard microphone measurements. In the 2.5 kHz band the blowing self noise drowns the airfoil self noise slightly, and parasitic sound sources appear at the upper and lower parts of the airfoil span, indicating that the mass flow rate of the ejected jet is not completely constant over the span. This was confirmed by HWA measurements and is subject of current investigations for further improvement.

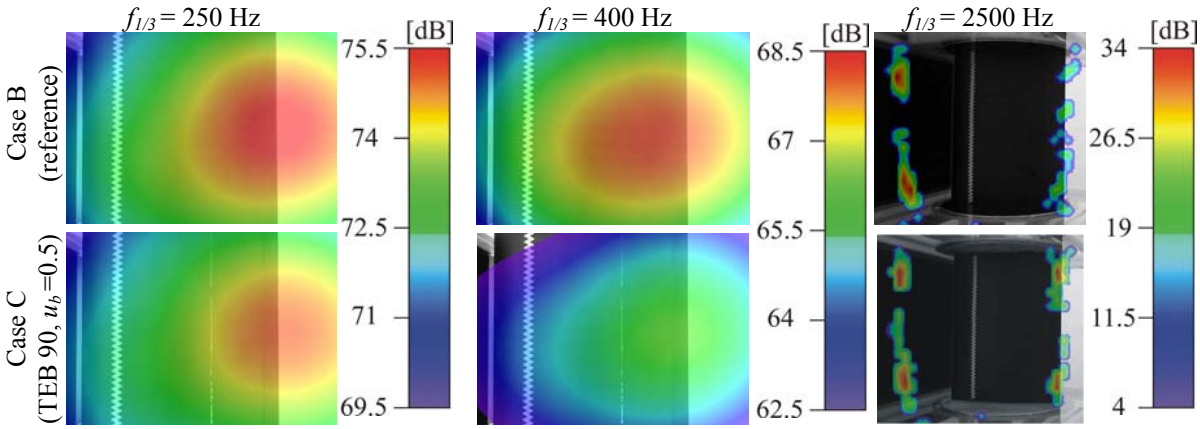

Figure 13. Microphone array measurements of the sound pressure level in the near field (left and middle) and far-field (right), data refer to different 1/3-octave frequency bands; view from suction side; different algorithms are applied for array data processing.

4. Conclusions

For mitigation of trailing edge noise (TEN) from a stationary airfoil section trailing edge blowing (TEB) was investigated. Three different TEB airfoils operating at a blowing rate of u_b = 0.5 were compared to an unmodified reference S834 airfoil.

Measurements and LES predictions showed that the blowing jet reduces the turbulence intensity in the TE region. Consequently, the induced low frequency surface pressure fluctuations are reduced by up to 10 dB. The acoustic measurements revealed dominant contributions from the TE from 160 Hz to at least 3 kHz. The peak TEN level appears in terms of a hump in the frequency spectrum around 500 Hz. In this frequency region the most advantageous TEB airfoil with the slot located at 90 % chord length showed a reduction of 3 dB at this particular blowing rate (u_b = 0.5). Of further interest is how TEB affects lift and drag of the airfoil. A former RANS study (not presented here) indicated that for most cases drag was decreased due to the momentum added to flow by the blowing jet, while lift remained nearly constant.

Variation and optimization of the blowing parameters in terms of blowing geometry and blowing rate are subject of ongoing investigations. An increase of the blowing rate may increase the sound at high frequencies due to the self noise from the blowing jets which, however, may be compensated partly by the favourable attenuation of high frequency sound in the atmosphere. Another issue to be covered is the up-scaling to realistic Reynolds numbers of the results found so far. LES, large wind tunnel and/or full scale turbine tests will show how reliable the findings presented here are.

References

[1] Roger M 2009 in *VKI LS 2009-03: Aerodyn. noise fr. wall-bounded fl.* ed Anthoine/Christophe
[2] Oerlemans S 2004 Subcontractor Report *NREL/SR-500-35339*
[3] Oerlemans S Sijtsma P Méndez and Lopéz B 2007 *J. of Sound and Vibration* **299** 869-883
[4] Blake W K and Gershfeld J L 1989 in *Frontiers in Exp. Fluid Mech.* ed Gad-el Hak M
[5] Shannon D W and Morris S C 2006 Exp Fluids **41** 777-788
[6] Geyer T Sarradj E and Fritzsche C 2010 *Exp. in Fluids* (Springer-Verlag) **48** (2) 291-308
[7] Finez A Jondeau E Roger M and Jacob M C 2010 *16th AIAA Aeroac. Conf.* AIAA 2010-3980
[8] Oerlemans S Fisher M Maeder T and Kögler K 2008 *14th AIAA Aeroac. Conf.* AIAA 2008-2819
[9] Herr M 2007 in *New Results in Num. and Exp. Fluid Mech. VI* **96** (Springer-Verlag) 430-437
[10] Tongchitpakdee C Benjanirat S and Sankar L N 2006 *J of Solar Eng.* **128** 432-444
[11] Shires A and Kourkoulis V 2013 *Energies* **6** (8) 3744-63
[12] Fite E B Woodward R P Podboy G G 2006 *3rd AIAA Flow Cont. Conf.* (USA) AIAA 2006-2844
[13] Winkler J Carolus T Scheuerlein J and Dinkelacker F 2010 *16th AIAA Aeroac. Conf.* AIAA 2010-3981
[14] Kohlhaas M Bamberger K Carolus T 2013 *19th AIAA Aeroac. Conf.* (Germany) AIAA 2013-2294
[15] Howe M S 2002 J of Sound and Vibration **249** (4) 679-700
[16] Somers D M 2005 Subcontractor Report *NREL/SR-500-36340*
[17] Brooks T F Marcolini M A and Pope D S 1984 *9th AIAA Aeroac. Conf.* (USA) AIAA-84-2266
[18] Drela M 1989 Low Reynolds Number Aerodynamics *Lecture Notes in Engineering* **54** 1-12
[19] Selig M S Ashok G Giguère P and Lyon C 2001 *Fixed and flapping wing aerodyn. for micro air vehicle applications* (AIAA) ed T J Mueller **195** 143-167
[20] Winkler J and Carolus T 2009 *Noise Control Engineering J.* **57** (4) 370-383
[21] Determination of sound power levels of noise sources using sound pressure-precision methods for anechoic and hemi-anechoic rooms 2003 *ISO 3745* (Geneva, Switzerland)
[22] Blake W K and Lynch D A 2002 *Aeroacoustic Measurements* ed T J Mueller (Springer-Verlag) 218-257
[23] Sijtsma P 2007 *13th AIAA/CEAS Aeroacoustic Conference* (Rome, Italy) AIAA-2007-3436
[24] Nicoud F Ducros F 1999 *Flow, Turbulence and Combustion* **62** 183-200
[25] Menter F 1994 *AIAA J.* **32** (8) 1598-1605
[26] Gerhard T Carolus T 2014 *21st Int. Congress on Sound and Vibr.* (Peking, China)